HHS Public Access

Author manuscript

Int J Med Eng Inform. Author manuscript; available in PMC 2015 November 10.

Published in final edited form as:

Int J Med Eng Inform. 2011 ; 3(3): 286–298. doi:10.1504/IJMEI.2011.042874.

Tissue Probability Map Constrained 4-D Clustering Algorithm for Increased Accuracy and Robustness in Serial MR Brain Image Segmentation

Zhong Xue[a,*], **Dinggang Shen**[b,†], **Hai Li**[a,c], and **Stephen Wong**[a]

[a] Department of Radiology, The Methodist Hospital Research Institute, Weill Cornell Medical College, Houston, TX

[b] Department of Radiology and Biomedical Research Imaging Center, University of North Carolina, Chapel Hill, NC

[c] School of Automation, Northwestern Polytechnical University, Xi'an, China

Abstract

The traditional fuzzy clustering algorithm and its extensions have been successfully applied in medical image segmentation. However, because of the variability of tissues and anatomical structures, the clustering results might be biased by the tissue population and intensity differences. For example, clustering-based algorithms tend to over-segment white matter tissues of MR brain images. To solve this problem, we introduce a tissue probability map constrained clustering algorithm and apply it to serial MR brain image segmentation, *i.e.*, a series of 3-D MR brain images of the same subject at different time points. Using the new serial image segmentation algorithm in the framework of the CLASSIC framework, which iteratively segments the images and estimates the longitudinal deformations, we improved both accuracy and robustness for serial image computing, and at the mean time produced longitudinally consistent segmentation and stable measures. In the algorithm, the tissue probability maps consist of both the population-based and subject-specific segmentation priors. Experimental study using both simulated longitudinal MR brain data and the Alzheimer's Disease Neuroimaging Initiative (ADNI) data confirmed that using both priors more accurate and robust segmentation results can be obtained. The proposed algorithm can be applied in longitudinal follow up studies of MR brain imaging with subtle morphological changes for neurological disorders.

1 Introduction

Image segmentation plays a key role in quantitative analysis of MR brain images of many medical imaging applications, such as morphometry, automatic tissue labeling, tissue/region quantification, image registration, and image-guided surgery [1, 2, 3, 4, 5, 6, 7, 8]. In image computing tasks such as analyzing normal development, aging, and neuro-degeneration, it is important to conduct follow up study and to quantify the subtle longitudinal morphological changes of MR brain images. In these studies, a series of 3-D images of the same subject are

*zxue@tmhs.org

†dgshen@unc.edu

usually captured at different time-points, and the focus is to quantitatively measure the morphological changes of the whole brain or a specific regions [9, 10, 11] across with time. Longitudinal stability is critical when measuring subtle subject changes with time, since true signal might be overwhelmed by the measurement errors if one processes the serial images individually. Existing 3-D segmentation and registration algorithms may not be able to provide sufficient power for longitudinal stability since they process each 3-D image separately. It is also a challenge when the presence of vascular or other pathologies changes signal characteristics, such as tissue contrast, thereby rendering tissue segmentation unreliable. In fact, it is particularly important to accurately align corresponding longitudinal anatomical structures and measure the subtle anatomical changes across different time points by using the temporal information provided in the 3-D image series. Recently, several 4-D image processing algorithms and joint segmentation and registration algorithms have been proposed [12, 13], and among which, we have proposed a method that overcomes this limitation and significantly improves longitudinal stability or temporal consistency of segmentation by formulating the segmentation problem in 4-D [14].

In [14], a novel algorithm for longitudinal MR brain image segmentation was proposed based on an extension of the FANTASM algorithm [15] by using additional temporal constraints forcing temporally corresponding voxels being segmented with the same tissue type, which we refer to as CLASSIC (Consistent Longitudinal Alignment and Segmentation for Serial Image Computing). CLASSIC not only jointly segments a series of longitudinal 3-D MR brain images of the same individual, but also estimates the longitudinal deformations in the image series, *e.g.* tissue atrophy. It iteratively performs two steps: i) jointly segment a series of 3-D images using a 4-D image-adaptive clustering algorithm based on the current estimate of the longitudinal deformations in the image series, and ii) refine these longitudinal deformations using a 4-D elastic warping algorithm [16, 17]. In this way, both a longitudinally-consistent segmentation and an estimate of longitudinal deformation of anatomy (*e.g.* atrophy) in a series of 3-D images can be estimated. The 4-D image-adaptive clustering algorithm used in CLASSIC extends the RFCM and FANTASM algorithms in three aspects. First, a new temporal consistency constraint term on the fuzzy membership functions is used in order to obtain temporally-consistent segmentation results. Second, the spatial and temporal constraints of the fuzzy membership functions are adaptive to the smoothness of the image, *i.e.* they are stronger in the regions that have more uniform image intensities, and vice versa. Thus the fuzzy membership functions are not necessarily overly smooth across tissue boundaries. Third, the clustering centers at each voxel location are adaptive to relatively local image intensity variations. In this way, the proposed 4-D clustering algorithm not only provides temporally-consistent segmentation results, but also adapts to local image intensity variations. If the image inhomogeneity has been corrected prior to applying CLASSIC, the clustering centers do not have to be spatially adaptive in order to improve the speed of the algorithm.

Since the size and intensities of different tissue classes vary greatly in different images and applications, the clustering results might be biased by the tissue population and intensity differences, as well as the spatial distribution of tissues or the anatomical structures. For example, most clustering-based algorithms tend to over-segment white matter tissues of MR

brain images. To solve this problem, we introduce a tissue probability map or segmentation prior constrained clustering algorithm and apply it to serial MR brain image segmentation. The tissue probability map consists of both the population-based and subject-specific segmentation priors. In this way, the clustering algorithm is not only driven by the image data but also constrained the probability of different tissue types of each image location, and increased segmentation accuracy and robustness is obtained. We then apply the new tissue probability constrained segmentation algorithm in the framework of the CLASSIC algorithm [14]. We therefore refer [14] as CLASSIC-I (with no tissue probability constraint) and the segmentation prior constrained method as CLASSIC-II.

Experiments are performed to segment both simulated and real longitudinal MR brain images. Both quantitative and visual comparisons are performed to compare the performance of CLASSIC with and without using the tissue probability maps, *i.e.*, CLASSIC-I and II. For the simulated images, first the statistical model-based deformable simulation [18] is used to simulate different subject images, and then the longitudinal atrophy at the temporal lobe of each subject image are simulated using the atrophy simulation algorithm [19]. Because the underlying deformation and the global and local volumes are known, the correct classification rates are calculated to quantitatively evaluate the accuracy of the proposed algorithm. Both CLASSIC-I and II are compared, and the results show that by using the tissue probability map, more accurate segmentation results can be obtained. Specifically, the new algorithm overcomes the disadvantage of over-segmentation of white matter for clustering-based image segmentation. For real images, the longitudinal 3-D T1-SPGR MR images of the Alzheimer's Disease Neuroimaging Initiative (ADNI) are used in the experiments. In all the experiments, we focused on evaluating the performance of the algorithms in terms of obtaining temporally-consistent segmentation, capturing global and local intensity/contrast changes, as well as estimating longitudinal deformations. The results on simulated datasets demonstrate that by using tissue probability maps in the clustering algorithm more accurate segmentation results can be obtained, and it is less biased by the spatial and intensity distribution of different tissues. The new segmentation algorithm for CLASSIC and the 4-D HAMMER registration algorithm are publicly available upon request.

The remainder of the paper is organized as follows. In Section 2, we introduce the tissue density map constrained CLASSIC algorithm in detail. Section 3 presents the experimental results, and Section 4 is the conclusion of this study.

2 Method

2.1 The Framework of the Algorithm

The CLASSIC algorithm [14] is a framework for longitudinal alignment and segmentation of MR brain images, and it jointly segments a 4-D image and follows the underlying temporal changes in anatomical structures, in order to provide more stable and consistent tissue segmentation. Particularly, the CLASSIC algorithm iteratively performs the following two steps: *i)* Given a current estimate of the longitudinal deformations necessary to align serial 3-D images, it jointly segments the image series using the 4-D fuzzy clustering algorithm. The major idea is that temporal consistent segmentation is achieved for

longitudinally corresponding tissues; *ii)* It refines the underlying longitudinal deformations using a traditional registration algorithm. Notice that any traditional registration algorithm that takes an initial deformation field and refines the registration result based on the segmented images in order to better match the input images can be easily embedded into this framework. In this paper, we used the 4-D elastic warping algorithm, the 4-D HAMMER algorithm [16]. In our CLASSIC software, we provide an interface so that different registration algorithms can be incorporated. In this paper, the tissue probability map constrained clustering algorithm is proposed below, please refer to [16, 14] for details about the registration and segmentation steps for CLASSIC.

2.2 The Tissue Probability Map Constrained 4-D Clustering Algorithm

2.2.1 Tissue Probability Map Constrained 4D Fuzzy Clustering Algorithm—In this paper, we propose a tissue probability map or segmentation prior constrained clustering algorithm and apply it to serial MR brain image segmentation. This new segmentation can be embedded into the framework of CLASSIC. In traditional clustering-based segmentation, since the size and intensities of different tissue classes vary greatly in different images and applications, the clustering results might be biased by the tissue population and intensity differences, as well as the spatial distribution of tissues or the anatomical structures. Herein, we propose to use the tissue probability map as an additional constraint of the clustering algorithm to overcome such disadvantages.

Given a series of images I_t, $t \in T$, $T = \{t_1, t_2, \ldots, t_Y\}$ and the underlying longitudinal deformations $F_{t_1 \to t}$, $t = t_2, \ldots, t_Y$, the goal of the 4-D segmentation is to classify the tissues into white matter, gray matter and CSF, and the segmented images are denoted as $I_t^{(\mathrm{seg})}$, $t \in T$. Since $F_{t_1 \to t}$ is the deformation from I_{t_1} to I_t, the corresponding point of a voxel i of image I_{t_1} will be point $F_{t_1 \to t}(i)$ in image I_t. For simplicity, we denote point $F_{t_1 \to t}(i)$ in image I_t as point (t, i), thus $x_{(t,i)}$ indicates the intensity of point (t, i). From the segmentation results of the images of a population or the serial images of a subject, we can globally align them onto the space of the serial images to be segmented and obtain the tissue probability maps $p_{(t,i),k}$, which reflect the probability or segmentation prior of point (t, i) belonging to class k. These prior information can then be used as an additional constraint in the fuzzy clustering algorithm to reduce the effect of biased segmentation results because of the population and tissue intensity differences. This new tissue probability map constrained 4-D clustering algorithm can be formulated by minimizing the following new objective function:

$$E(\mu, c) = \frac{1}{2} \sum_{t \in T} \sum_{i \in \Omega(t_1)} \sum_{k=1}^{K} \{\mu_{(t,i),k}^2 (x_{(t,i)} - c_{t,k})^2 + \gamma (\mu_{(t,i),k} - p_{(t,i),k})^2 + \alpha \mu_{(t,i),k}^2 \overline{\mu}_{(t,i),k}^{(s)} + \beta \mu_{(t,i),k}^2 \overline{\mu}_{(t,i),k}^{(t)}\}, \quad (1)$$

where voxel $x_{(t,i)}(t \in T, i \in \Omega(t_1))$ is classified into different tissue types by finding the clustering centers $c_{t,k}$, the kth clustering center of image I_t, and $\mu_{(t,i),k}$, the fuzzy membership function of $x_{(t,i)}$ belonging to class k. The first term in Eq.(2) is the standard energy term for fuzzy clustering algorithm. The second term reflects the constraint of the tissue probability maps and γ is the weight for the constraint. The third and the forth terms are the spatial and the temporal segmentation consistency constraints along the longitudinal deformations, and

a and β are the weights, respectively. $\overline{\mu}^{(s)}_{(t,i),k}=\frac{1}{N_1}\sum_{(t,i)\in N^{(s)}_{(t,i)}}\sum_{m\in M_k}\mu^2_{(t,i)m}$, and $\overline{\mu}^{(t)}_{(t,i),k}=\frac{1}{N_2}\sum_{(t,i)\in N^{(t)}_{(t,i)}}\sum_{m\in M_k}\mu^2_{(t,i),m}$, where $N^{(s)}_{(t,i)}$ is the spatial neighborhood of point (*t*, *i*), $N^{(t)}_{(t,i)}=\{(\tau,i):|\tau-t|\leq T_N\}$ is the temporal neighborhood of point (*t*, *i*) along the temporal deformation, and N_1 and N_2 are the numbers of addends for normalization. These spatial and temporal consistency constraints are designed by following the formulation in the FANTASM algorithm.

The fuzzy membership functions are subject to

$$\sum_{k=1}^{K}\mu_{(t,i),k}=1,\ \text{for all}\, i\in\Omega(t_1), t\in T. \quad (2)$$

It can be seen that the algorithm becomes CLASSIC (with no spatial adaption for clustering centers) when $\gamma = 0$, it is similar to the Robust FCM algorithm [20] when $\gamma = 0$ and $\beta = 0$, and it becomes the standard FCM algorithm when $a = 0$, $\beta = 0$, and $\gamma = 0$. Therefore, by setting properly the parameters a, β, and γ, we can apply constraints on spatial smoothness, temporal consistency, and prior tissue knowledge on the 4-D clustering algorithm.

Using Lagrange multipliers to enforce the constraint in Eq.(2), and calculating its partial derivatives with respect to *mu* and *c*, we can get the equations to iteratively update them:

$$\mu_{(t,i),k}=\left(\frac{1-\sum_{l=1}^{K}\{\gamma p_{(t,i),l}g^{-1}_{(t,i),l}\}}{\sum_{l=1}^{K}g^{-1}_{(t,i),l}}+\gamma p_{(t,i),k}\right)\cdot g^{-1}_{(t,i),k}, t\in T, i\in\Omega(t_1), \quad (3)$$

where $g_{(t,i),k}=(x_{(t,i)}-c_{t,k})^2+\gamma+\alpha\overline{\mu}^{(s)}_{(t,i),k}+\beta\overline{\mu}^{(t)}_{(t,i),k}$, and the equation to update the centroids can be acquired,

$$c_{t,k}=\frac{\sum_{i\in\Omega(t_1)}\mu^2_{(t,i),k}x_{(t,i)}}{\sum_{i\in\Omega(t_1)}\mu^2_{(t,i),k}}. \quad (4)$$

The 4D clustering algorithm can be summarized as follows: *(1)* Set a, β, γ, and neighborhoods $N^{(s)}_{(t,i)}$ and $N^{(t)}_{(t,i)}$, segment each image using FCM and thus we get the initial clustering centers $c_{t,k}$; *(2)* Compute fuzzy membership functions using Eq.(3); *(3)* Compute centroids using Eq.(4); *(4)* If the algorithm converges (the difference of the values of the objective function between two iterations is smaller than a prescribed threshold), then output the segmentation results, otherwise go back to step *(2)*. Similar to the standard FCM algorithm, the new algorithm usually converges after 10 to 30 iterations dependent on the difference values to terminate the iteration.

2.3 Estimation of Tissue Probability Maps

In the previous section, we have introduced that the tissue probability maps $p_{(t,i),k}$ are used as a constraint in the 4-D segmentation algorithm. In this section, we explain how they are calculated in detail. In this work, a tissue probability map consists of the one calculated from the segmentation results of a population and the one calculated from some 3-D segmentation of the serial images of the subject.

2.3.1 Population-based segmentation priors—In order to obtain the population-based segmentation priors, all the S sample images captured from a population are segmented using a 3-D segmentation algorithm [21], and then all these segmented images are linearly aligned onto the space of the template image I_{temp}. Denoting $n^{\text{temp}}(i, k)$ as the number of linearly aligned sample images whose voxel i is segmented as tissue k, the segmentation prior of class k at voxel i is defined as,

$$p_{i,k}^{\text{temp}} = \frac{n^{\text{temp}}(i,k)}{S}, \quad i \in \Omega_{\text{temp}}, \quad k = 1, \ldots, K, \quad (5)$$

where Ω_{temp} is the space of the template image, and $\sum_{k=1}^{K} p_{i,k}^{\text{temp}} = 1$. When applying the population-based segmentation prior onto a series of input images I_t, $t = t_1, \ldots, t_Y$, we can globally transform the segmentation priors $p_{i,k}^{\text{temp}}$ onto the space of the first image I_{t_1} by using the linear transformation that aligns the template image I_{temp} onto I_{t_1}. Herein, the FSL flirt toolkit is applied in order to globally align the images. We denote these linearly transformed priors as $p_{i,k}^{\text{pop}}$, which reflect the knowledge learned from S samples of a population, where $i \in \Omega(t_1)$ is defined in the space of the first image.

2.3.2 Subject-specific segmentation priors—Similar with the population-based priors, we can get the subject-specific segmentation priors using the segmentation results of the serial images under consideration. Initially, since the segmentation results are not available, the 3-D segmentation algorithm [21] is used to segment the image individually, and in the following iterations, the current segmentation results are used to calculate the subject-specific priors. The subject-specific priors can be obtained by first globally aligning them onto the space of the first time point image and then calculating,

$$p_{i,k}^{\text{sub}} = \frac{n^{\text{sub}}(i,k)}{Y}, \quad i \in \Omega_{t_1}, \quad k = 1, \ldots, K, \quad (6)$$

where Y is the number of the serial images, and $n^{\text{sub}}(i, k)$ is the number of the serial images whose voxel i is segmented as tissue k.

2.3.3 Combining priors—The overall segmentation priors can be expressed as the combination of the population-based and the subject-specific priors using a weighting coefficient ξ,

$$p_{i,k}=\xi p_{i,k}^{\text{pop}}+(1-\xi)p_{i,k}^{\text{sub}},\ 0\le\xi\le 1. \quad (7)$$

Notice that $p_{i,k}$ is defined on the space of the first image, *i.e.* $i \in \Omega(t_1)$. Therefore, the segmentation priors at point (t, i) is $p_{(t,i),k} = p_{i,k}$, $t = t_1, \ldots, t_Y$. In this paper we set ξ as 0.7.

3 Results

3.1 Experiments on Simulated Longitudinal Data

Using the statistical simulation algorithm [18] from a template image, we first simulated 10 new MR brain images acting as the first time point image of different subjects, and then simulated serial images of each simulated subject image using the atrophy/growth simulation package [19]. In this way, the ground truth of the tissue types and the longitudinal deformations of the serial images are known. Notice that the template image is also a simulated image: we added spatially correlated Gaussian noises to an already segmented image, and the mean intensities of white matter, gray matter and CSF are 45, 85, and 110, respectively, and the standard deviation of the Gaussian noise is set to 15. Both the two CLASSIC versions are used to process the simulated serial images, and the only difference between the two algorithms is that one uses the tissue probability map as an additional constraint and another not. In the experiments, we used the same program, while setting the parameter γ to zero to discard the constraint of the tissue probability maps. The tissue probability maps are calculated using the method described in Section 2.3, and the 3-D segmentation results by applying FANTASM. The population-based priors are calculated by applying HAMMER [17] to align all the MR brain images in this study to the template image space, and the FSL linear transformation is used to align all the tissue probability maps onto the space of the first time point image.

Fig. 1 shows the template image and 3 simulated subject images. Using the statistical model-based deformation simulation [18], various realistic anatomical shapes of MR brain images can be simulated. The second row in Fig. 1 gives the corresponding simulated segmented images of them. The simulated longitudinal data will be generated based on these segmented images which act as the ground truth of the segmentation. From each of the simulated subject image, we manually select a point within the temporal lobe and simulate a gradual atrophy of a spherical region around that point across with time. For each subject image, five time point images are simulated, and Fig. 2 gives an example of the simulated serial images. Notice that atrophy on left temporal lobe region (circled) is gradually introduced. The population-based tissue probability maps are shown in Fig. 3 (top), and Fig. 3 (bottom) illustrates the subject-specific tissue probability maps of the subject shown in Fig. 2.

We applied both CLASSIC-I and II for segmenting the above 10 simulated serial image datasets. Both the volumes and the correct classification rate (CCR) can be calculated for each segmentation result with respect to the ground truth within a volume of interest. Herein, we calculated the white matter and gray matter volumes, as well as the CCR for all the images within the previously selected spherical regions, and Fig. 4(a) shows the mean and standard deviation of the volumes, and Fig. 4(b) gives the correct classification rates for different subjects across different time points. It can be seen that i) in terms of local volume

measures, both versions obtained very similar volumetric measures as compared to the ground truth, however in terms of CCR, the CLASSIC with tissue probability maps is better: with higher CCR values. These results indicate that since the white matter and gray matter are combined together in the volumetric measure, there might be some difference in the segmentation results for different tissues since the total volumes are similar but the CCRs are different. In fact if calculating the volumes for white matter and gray matter separately (see Fig. 5), we can immediately see the difference of the two versions and the results indicate that by using the tissue probability maps, the clustering results overcomes the disadvantage of over-segmentation of white matter tissues, thus providing more accurate segmentation.

3.2 Experiments on Analyzing Longitudinal Images of Alzheimer's Disease

We applied the algorithm to ADNI (www.loni.ucla.edu) data. The ADNI was launched in 2003 by the National Institute on Aging (NIA), the National Institute of Biomedical Imaging and Bioengineering (NIBIB), the Food and Drug Administration (FDA), private pharmaceutical companies and non-profit organizations, as a $60 million, 5-year public-private partnership. The primary goal of ADNI has been to test whether serial magnetic resonance imaging (MRI), positron emission tomography (PET), other biological markers, and clinical and neuropsychological assessment can be combined to measure the progression of mild cognitive impairment (MCI) and early Alzheimer's disease (AD). Determination of sensitive and specific markers of very early AD progression is intended to aid researchers and clinicians to develop new treatments and monitor their effectiveness, as well as lessen the time and cost of clinical trials. The Principle Investigator of this initiative is Michael W. Weiner, M.D., VA Medical Center and University of California, San Francisco. ADNI is the result of efforts of many co-investigators from a broad range of academic institutions and private corporations, and subjects have been recruited from over 50 sites across the U.S. and Canada. The initial goal of ADNI was to recruit 800 adults, ages 55 to 90, to participate in the research – approximately 200 cognitively normal older individuals to be followed for 3 years, 400 people with MCI to be followed for 3 years, and 200 people with early AD to be followed for 2 years. For up-to-date information see www.adni-info.org. In the future, we plan to apply the proposed algorithm to calculate the temporal morphological changes for all the subjects and compare its results with the current SPM-based volumetric measures for each region of interest of the whole brain. The major goal will be to obtain stable longitudinal measure in order to obtain the subtle morphological changes and their differences for normal aging, MCI and AD.

Data collection and sharing was funded by the Alzheimers Disease Neuroimaging Initiative (ADNI; Principal Investigator: Michael Weiner; NIH grant U01 AG024904). ADNI is funded by the National Institute on Aging, the National Institute of Biomedical Imaging and Bioengineering (NIBIB), and through generous contributions from the following: Pfizer Inc., Wyeth Research, Bristol-Myers Squibb, Eli Lilly and Company, GlaxoSmithKline, Merck & Co. Inc., AstraZeneca AB, Novartis Pharmaceuticals Corporation, Alzheimers Association, Eisai Global Clinical Development, Elan Corporation plc, Forest Laboratories, and the Institute for the Study of Aging, with participation from the U.S. Food and Drug Administration. Industry partnerships are coordinated through the Foundation for the

National Institutes of Health. The grantee organization is the Northern California Institute for Research and Education, and the study is coordinated by the Alzheimers Disease Cooperative Study at the University of California, San Diego. ADNI data are disseminated by the Laboratory of Neuro Imaging at the University of California, Los Angeles.

In this preliminary test, we applied the algorithm to 25 ADNI datasets (MCI), and the goal is to evaluate the performance of the algorithm on real data. For all the original MR brain data, the FSL BET skull stripping program has been used to remove the skulls, and some mannual correction is conducted for some larger regions that have not been removed. Then, the FANTASM segmentation algorithm was used to segment the images in 3-D, and the segmentation results were used as the initial subject-specific tissue probability maps in the CLASSIC-II. In order to quantitatively analyze the segmentation results, we used a Temporal Consistency (TC) factor to reflect the temporal consistency of the segmentation results. Suppose $x^{\text{seg}}_{(t,i)}$ is the segmentation result (label) of $x_{(t,i)}$, the segmentation results of voxel i across different times can be denoted as $x^{\text{seg}}_{(t_1,i)}, x^{\text{eg}}_{(t_2,i)}, \ldots, x^{\text{seg}}_{(t_Y,i)}$. Denote L_i as the number of label changes of corresponding voxels across time, then the segmentation of the corresponding voxels is consistent if L_i is small, and vice versa. Therefore, the TC of segmentation results is measured by $TC = 1/S(\Omega') \sum_{i\in\Omega'} (1 - L_i/(Y-1))$, where Ω' is the voxel set of the region of interest, and $S(\Omega')$ is the number of voxels in Ω'. Both the TC values obtained from 3-D segmentation and CLASSIC-II are calculated and shown in Fig. 7(a). Notice that longitudinal deformations among the serials images are needed in order to calculate the TC values. For 3-D segmentation results, we applied the 3-D hierarchical volumetric image registration [17] to obtain them, and for CLASSIC-II, both the longitudinal deformations and the 4-D segmentation results can be obtained simultaneously. It can be seen from the figure that the TC values for 4-D algorithm are much higher than those of 3-D, indicating that longitudinally stable segmentation and alignment of serial images is achieved. Moreover, we also calculated the volumes of interest (a spherical region within the left temporal lobe) and plotted the mean and standard deviations of such volumes for all the 25 image series. Notice that the scanning time and age information had not been used in calculating such values across different subjects. The purpose here is to show whether we can obtain the stable temporal volumetric changes for a number of subjects. The results are shown in Fig. 7(b), and it can be seen that a steady volumetric decrease has been found from these subjects (1.5% in terms of volumes).

Notice that the traditional quantitative image computing algorithms first segments the images and then performs image registration, and the registration results rely on the segmentation of individual image, and hence there is no mechanism to refine the segmentation and registration results. The proposed method iteratively registers and segments images. In this way, the registration algorithm could have better ability to refine the results and converge to acceptable or better registration results. The underlying assumption is that the majority of the image voxels is registered and segmented correctly during the first iteration, and thus the initializations of the registration in the following iterations are close to the solution in order to make sure the iterative procedure is stable. Since the proposed tissue probability map constrained 4-D segmentation algorithm has been applied in the CLASSIC framework, which iteratively refines the segmentation and the

longitudinal deformation. It is important to investigate how this iterative procedure converges. We therefore performed the algorithm for a series of real MR brain images and calculated the TC values of the segmentation results obtained from different iterations. Fig. 8 shows the results. It can be seen that initially the TC value for such image series is 78.8% (this is based on the 3-D segmentation), and after one iteration the TC values increased to 85.3%, and the TC values tend to be quite stable for the following iterations. Therefore, the proposed iterative procedure converges very fast, and we performed 2 iterations in all the experiments.

4 Conclusion

This paper proposed a tissue probability map constrained 4-D image segmentation algorithm for longitudinal image analysis. The algorithm iteratively estimates the longitudinal deformations among the image series that reflect the underlying structural changes across time and jointly segments the serial images. By using the tissue probability map as an additional constraint in the clustering algorithm, more accurate and robust segmentation results can be obtained for serial images. Experiments with simulated MR brain images and the ADNI data have confirmed the advantages of this algorithm.

References

1. Bezdek J, Hall L, Clarke L. Review of MR image segmentation techniques using pattern recognition. Medical Physics. 1993; 20(4):1033–1048. [PubMed: 8413011]
2. Pappas T. An adaptive clustering algorithm for image segmentation. IEEE Trans on Signal Processing. 1992; 40(4):901–914.
3. Udupa J, Samarasekera S. Fuzzy connectedness and object definition: theory, algorithms and applications in image segmentation. Graph Models Images Processing. 1996; 58(3):246–261.
4. Brandt M, Bohan T, Kranmer L, Fletcher J. Estimation of CSF, white and gray matter volumes in hydrocephalic children using fuzzy clustering of MR images. Comput Med Imag Graph. 1994; 18:25–34.
5. Lim K, Prefferbaum A. Segmentation of MR brain images into cerebrospinal fluid, white and gray matter. Journal of Comput Assisted Tomogr. 1989; 13:588–593.
6. Pham D, Prince J. Adaptive fuzzy segmentation of magnetic resonance images. IEEE Trans on Medical Imaging. 1999; 18(9):737–752. [PubMed: 10571379]
7. Chen, W.; Giger, M. A fuzzy c-mean (FCM) based algorithm for intensity inhomogeneity correction and segmentation of MR images. IEEE International Symposium on Biomedical Imaging (ISBI 2004); Arlington, VA. 2004. p. 1307-1310.
8. Rezaee M, van der Zwet P, Lelieveldt B, van der Geest R, Reiber J. A multiresolution image segmentation technique based on pyramidal segmentation and fuzzy clustering. IEEE Trans on Image Processing. 2000; 9(7):1238–1248.
9. Resnick S, Goldszal A, Davatzikos C, Golski S, Kraut M, Metter E, Bryan R, Zonderman A. One-year age changes in MRI brain volumes in older adults. Cerebral Cortex. 2000; 10:464–472. [PubMed: 10847596]
10. Tang Y, Whitman G, Lopez I, Baloh R. Brain volume changes on longitudinal magnetic resonance imaging in normal older people. Journal of Neuroimaging. 2001; 11(4):393–400. [PubMed: 11677879]
11. Freeborough P, Fox N. The boundary shift integral: an accurate and robust measure of cerebral volume changes from registered repeat MRI. IEEE Trans on Medical Imaging. 1997; 16(5):623–629. [PubMed: 9368118]
12. Wang, F.; Vemuri, B. MICCAI 2005. Palm Springs, CA: Springer; 2005. Simultaneous registration and segmentation of anatomical structures from brain MRI.

13. Chen, X.; Brady, M.; Lo, J.; Moore, N. IPMI 2005. Glenwood Springs, CO: Springer; 2005. Simultaneous segmentation and registration of contrast-enhanced breast MRI.
14. Xue Z, Shen D, Davatzikos C. CLASSIC: Consistent longitudinal alignment and segmentation for serial image computing. NeuroImage. 2006; 30:388–399. in press. [PubMed: 16275137]
15. Pham P, Prince J. Fantasm: Fuzzy and noise tolerant adaptive segmentation method. http://iacl.ece.jhu.edu/projects/fantasm/, (www)
16. Shen D, Davatzikos C. Measuring temporal morphological changes robustly in brain MR images via 4-D template warping. NeuroImage. 2004; 21(4):1508–1517. [PubMed: 15050575]
17. Shen D, Davatzikos C. HAMMER: Hierarchical attribute matching mechanism for elastic registration. IEEE Transactions on Medical Imaging. 2002; 21(11):1421–1439. [PubMed: 12575879]
18. Xue Z, Shen D, Karacali B, Stern J, Rottenberg D, Davatzikos C. Simulating deformations of mr brain images for validation of atlas-based segmentation and registration algorithms. NeuroImage. 2006; 33(3):855–866. [PubMed: 16997578]
19. Karacali B, Davatzikos C. Simulation of tissue atrophy using a topology preserving transformation model. IEEE Trans on Medical Imaging. 2005 under review.
20. Pham, P.; Prince, J. Robust unsupervised tissue classification in mr image. Proceedings of the 2004 IEEE International Symposium on Biomedical Imaging: Macro to Nano; Arlington, VA. 4 2004; p. 109-112.
21. Yan, M.; Karp, J. An adaptive bayesian approach to three-dimensional MR image segmentation. Conference on Information Process in Medical Imaging; 1995.

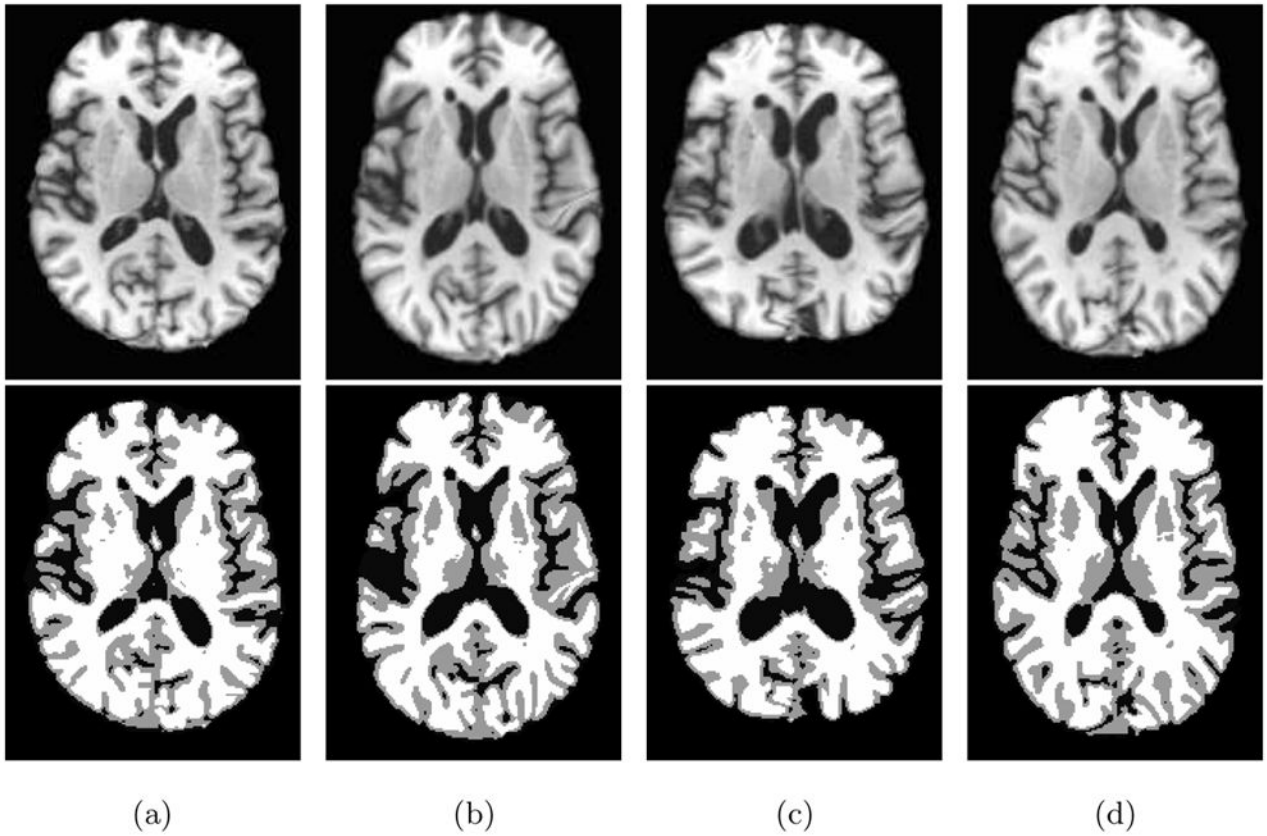

Figure 1.
The template image (a) and three sample simulated subject images (b,c,d).

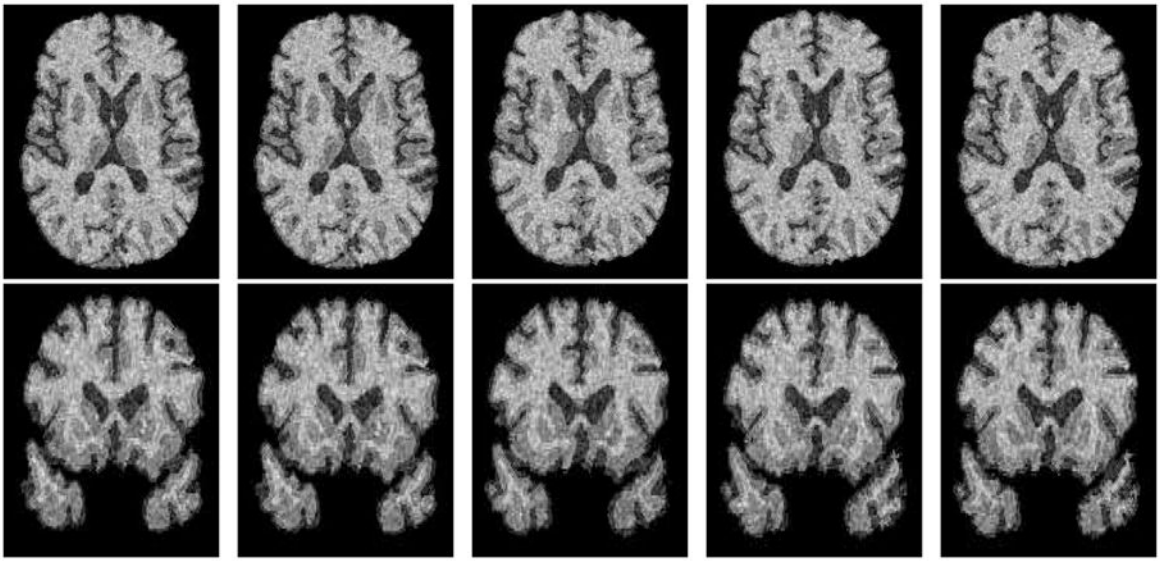

Figure 2.
A series of simulated images.

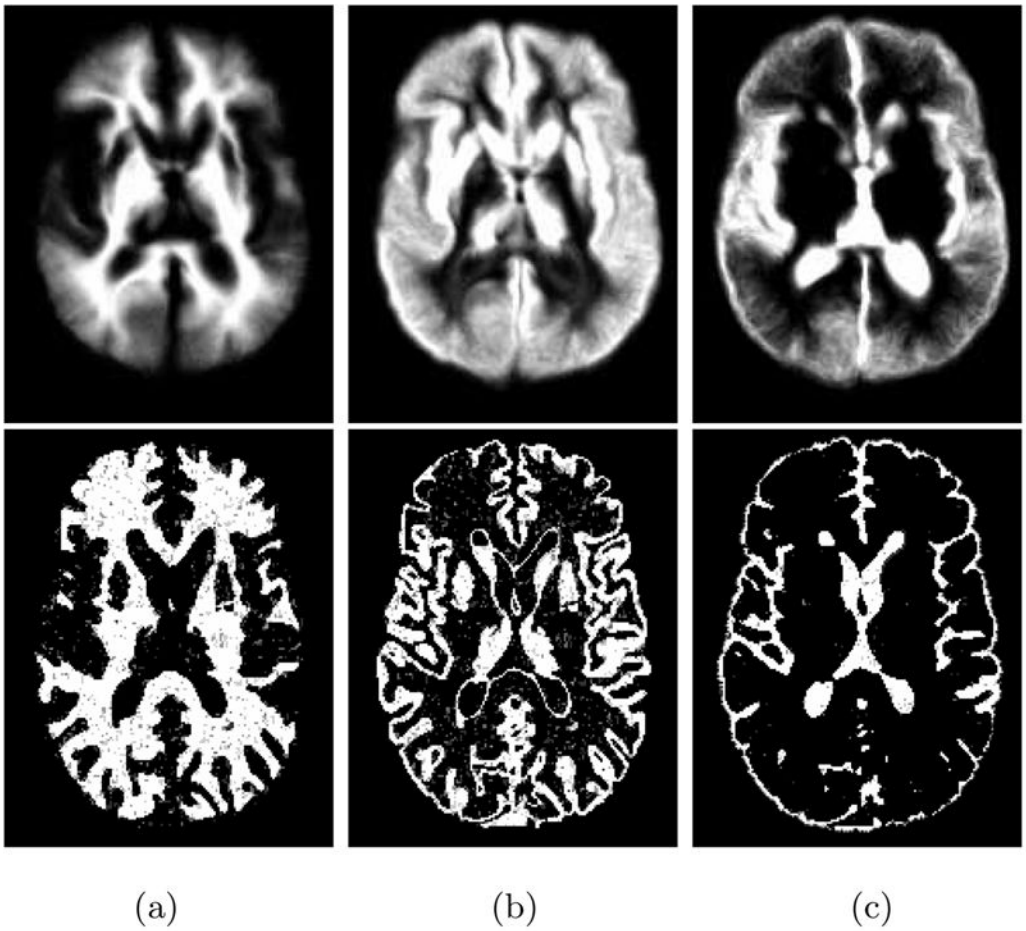

Figure 3.
The population-based segmentation priors (top) and the subject-specific segmentation priors (bottom, the subject is shown in Fig. 2) for WM (a), GM (b) and CSF (c), respectively. Notice that the population-based segmentation priors are in the template image space and will be affine transformed onto the first timepoint image, and the subject-based segmentation priors are in the space of the first timepoint image.

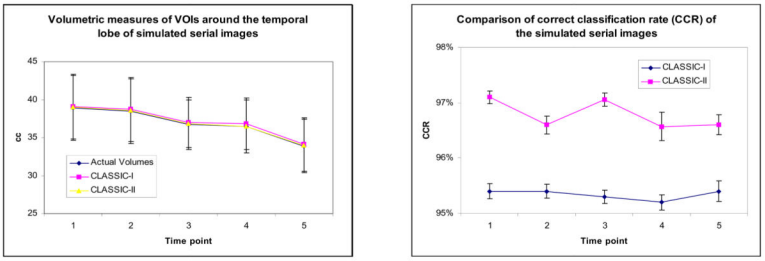

(a) (b)

Figure 4.

The mean and standard deviation values of the local volumes and the correct classification rates (CCR) in side a spherical neighborhood manually drawn in the temporal lobe, for 10 simulated series of images.

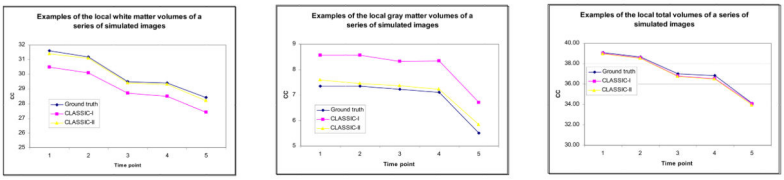

(a) (b) (c)

Figure 5.

The volumes of GM (a), WM (b) and GM+WM (c) are plotted for one series of images. It can be seen that by using the tissue probability map as an additional constraint, CLASSIC-II overcomes the problem for over-segmentation of white matter and improves the accuracy for gray matter and white matter

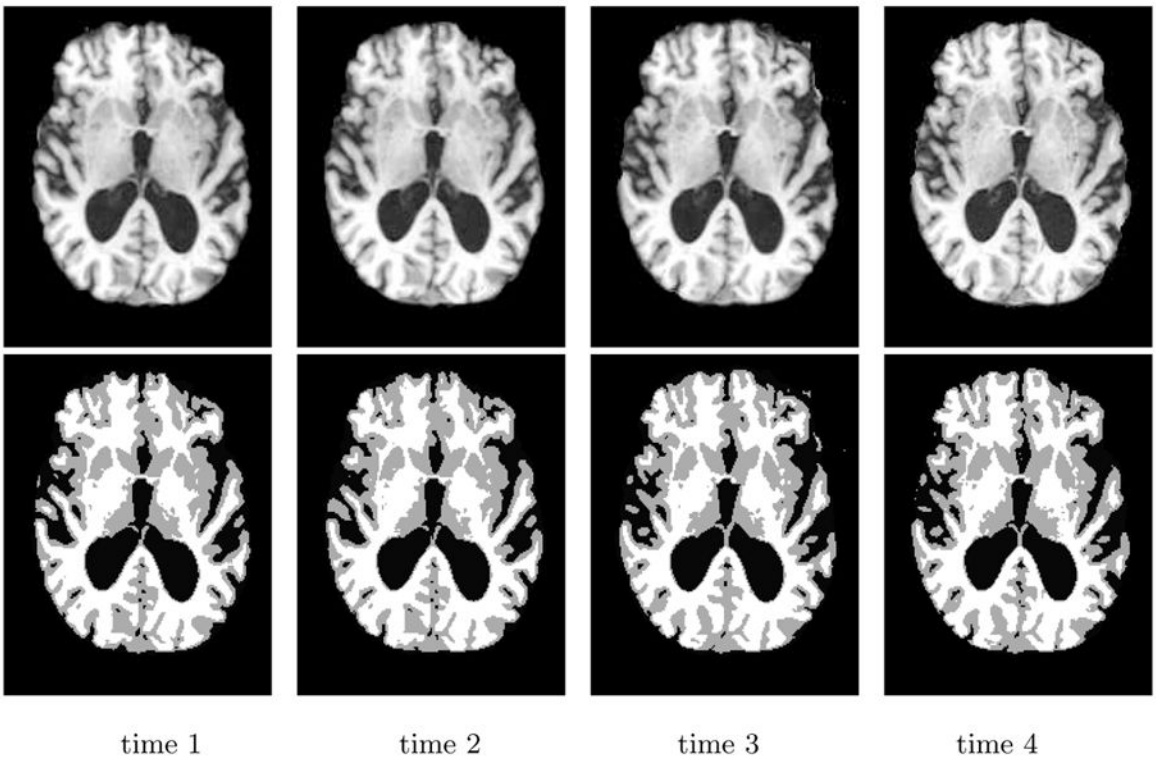

Figure 6.
An example of the 4-D segmentation of the ADNI data.

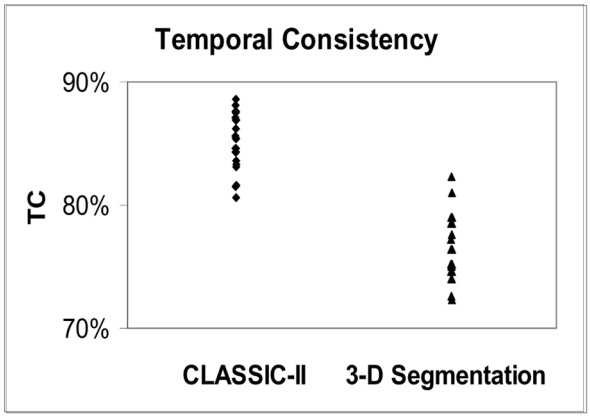

(a)

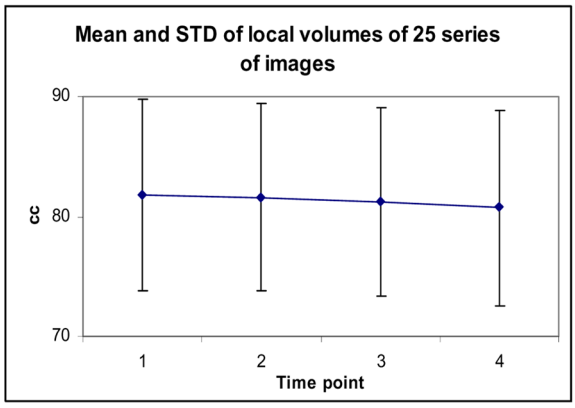

(b)

Figure 7.

Local volume measures and temporal consistency for real MR brain images. (a) The mean and standard deviation values of the local volumes of the spherical regions os temporal lobe for 25 subjects. The results indicates a steady volume decrease for the left temopral lobe; (b) The temporal consistency values for all the subjects calculated by the CLASSIC-II and 3-D segmentation (FAST). The results show that because of the use of the temporal deformations of the serial images, the segmentation of longitudinally corresponding tissues is more stable using the proposed algorithm.

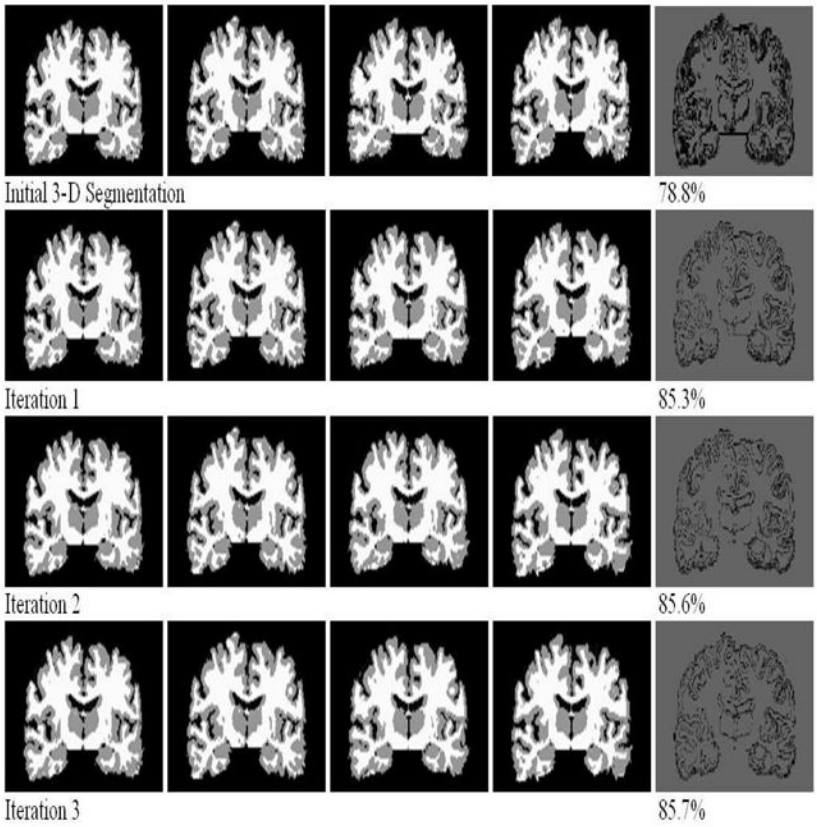

Figure 8.

Illustration of the TC of CLASSIC-II at different iterations. The right column shows the TC maps at different voxel on the template space, and the average TC values are given for each case.